Photophysical properties of 1,2,3,4,5-pentaarylcyclopentadienyl hydrotris(indazolyl)borate ruthenium(II) complexes

Sheng Gao, Yohan Gisbert, Guillaume Erbland, Seifallah Abid, Claire Kammerer, Alessandro Venturini, Gwénaël Rapenne, Barbara Ventura, Nicola Armaroli

Photophysical properties of 1,2,3,4,5-pentaarylcyclopentadienyl hydrotris(indazolyl)borate ruthenium(II) complexes

Sheng Gao,[a] Yohan Gisbert,[b] Guillaume Erbland,[b] Seifallah Abid,[b] Claire Kammerer,[b] Alessandro Venturini,[a] Gwénaël Rapenne,[b,c]* Barbara Ventura,[a]* Nicola Armaroli [a]

a. Istituto per la Sintesi Organica e la Fotoreattività, Consiglio Nazionale delle Ricerche (CNR-ISOF), Via Gobetti 101, 40129 Bologna, Italy. E-mail: barbara.ventura@isof.cnr.it

b. CEMES, Université de Toulouse, CNRS, 29 rue Marvig, F-31055 Toulouse Cedex 4, France. E-mail: rapenne@cemes.fr

c. Division of Materials Science, Nara Institute of Science and Technology, NAIST, 8916-5 Takayama-cho, Ikoma, Nara 630-0192, Japan.

Abstract

The photophysical properties of heteroleptic rotor-like Ru(II) complexes containing both a cyclopentadienyl-type ligand and a hydrotris(indazolyl)borate chelating unit with a piano stool structure (**Ar_5L1-Ru-S1** and **L3-Ru-S1**) and their corresponding subunits have been investigated. The complexes show peculiar absorption features if compared with those of their related ligands or fragments. **L3-Ru-S1** was found to be non-emissive, while **Ar_5L1-Ru-S1** shows a weak emission with quantum yield of 0.27%. With the support of DFT calculations, we demonstrate that the new absorption features can be attributed to ruthenium–based charge transfer transitions which involve the π* orbitals of the phenyl substituents of the cyclopentadienyl ligand.

Preprint

Submitted to *Phys. Chem. Chem. Phys.*

INTRODUCTION

Molecular machines are chemical systems that can undergo mechanical movement on the nanometric scale, upon application of a suitable external stimulus.[1] They can occur in living organisms, but can also be synthesised as so-called artificial molecular machines,[2] which are potentially relevant for applications in nanoscience,[3] biomedicine[4] and material science[5] and have been recently recognised with the Nobel Prize awarded to Sauvage, Stoddart and Feringa.[6] According to the type of movement in spatial dimension, they are classified as linear[7] (e.g., muscle fibers) or rotary[8] (e.g., ATP synthase). Due to their specific movement and structure, some of the rotary machines can be considered as molecular motors[9] or molecular gears.[10]

Among artificial molecular machines, only a few are based on coordination complexes even if this is a very versatile and efficient way to assemble mechanical subunits, allowing for the production of a large and diverse range of molecular machines thanks to the vast number of metals and ligands available to tune their molecular architectures and physico-chemical properties.[11]

In recent years, gear-shaped molecules have attracted considerable attention from synthetic and physical chemists.[12] In previous work, some of us designed, synthesised and rotated, thanks to the STM tip operating as electron provider[13] or electric-field inducer,[14] a series of star-shaped molecular motors and gears based on ruthenium complexes containing the hydrotris(indazolyl)borate ligands as tripodal platforms.[15] These compounds interestingly exhibited controlled clockwise or anticlockwise unidirectional rotation once anchored on metallic surfaces

As tiny movable entities, molecular machines can be stimulated, by chemical, electrical or optical inputs. The latter are preferable because particularly clean, effective, easy to operate and non-invasive.[16] Therefore, it is of capital importance to investigate the photophysical properties of the rotor elements to fully rationalise their mechanical behaviour under illumination.

In this work, we present a detailed investigation into the photophysical properties of two rotor-like Ru(II) complexes, **Ar$_5$L1-Ru-S1** and **L3-Ru-S1**,[17] along with their related ligands/fragments, in tetrahydrofuran (THF) solution both at 298 and 77 K (Scheme 1). In such complexes the metal is coordinated to a hydrotris(indazolyl)borate ligand and a penta(*p*-bromophenyl)cyclopentadienyl ligand or a penta(*m*-dimethylphenyl)cyclopentadienyl ligand respectively.[18] Model **L3-Ru-(CO)$_2$Br** is taken as a reference complex for **L3-Ru-S1** bearing only the cyclopentadienyl platform and lacking the scorpionate tripodal unit. **L1H**, **L2H** and **L3Br** are models for the pentaarylcyclopentadienide ligands, as they possess a central cyclopentadiene unit and different substituents on both the peripheral phenyls and the central ring. Finally, **S1K** and **S1Tl** are suitable models for the scorpionate tripodal hydrotris(indazolyl)borate ligand, differing only in the counterion, i.e., K^+ in **S1K** and Tl^+ in **S1Tl**.

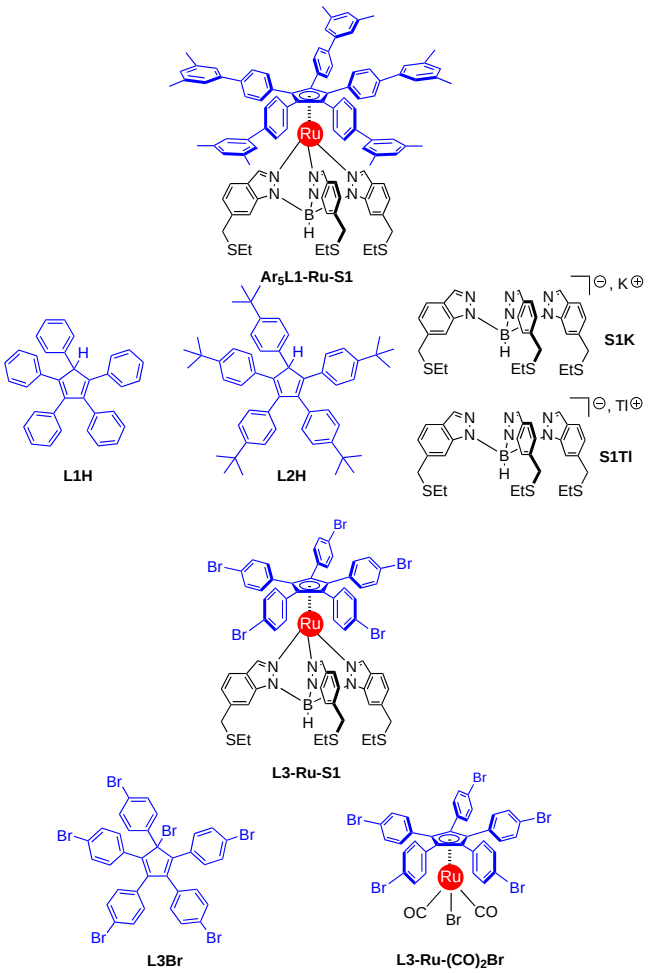

Scheme 1. *Structures of the two molecular rotors* ***Ar$_5$L1-Ru-S1*** *and* ***L3-Ru-S1****, along with their related ligands or fragments.*

The ligand geometry of these Ru(II) complexes is unique. Numerous studies on the photophysical properties of ruthenocene and cyclopentadienyl/arene Ru(II) complexes are reported in the literature[19] and show that these compounds are characterised by a weak and structured emission detectable only at low temperature. On the other hand, some examples of tris(1-pyrazolyl)methane based Ru(II) complexes have been explored, where the tripodal unit is one of the coordinating ligands, accompanied by 2,2'-bipyridine, pyridine or 1,10-phenanthroline type ligands.[20] These compounds exhibit from weak to intense luminescence at room temperature, in solution and in the solid state, generally attributed to a MLCT transition not involving the tripodal ligand. To the best of our knowledge, there are no reports on the photophysical behaviour of heteroleptic Ru(II) complexes containing both a cyclopentadienyl-type ligand and a hydrotris(indazolyl)borate chelating unit.

We report here a comprehensive photophysical analysis of the present systems, supported by theoretical studies, which is of key importance for the development of molecular rotors based on indazolyl-borate ligands that can be operated by light stimuli or which may exhibit useful photoinduced functions. Notably, this study covers the photophysics of an unusual class of Ru(II) complexes, bearing cyclopentadienyl and indazolyl ligands.

RESULTS AND DISCUSSION

Synthesis of the ligands and complexes

The synthesis of all compounds studied in this paper (Scheme 1) has been previously described. The tripodal thioether-functionalised hydrotris(indazolyl)borate ligands have been prepared as their potassium or thallium salts (**S1K** and **S1Tl**).[21] The complex **L3-Ru-S1** was synthesised by reaction of **S1Tl** with bromidodicarbonyl[η^5-1,2,3,4,5-pentakis(*p*-bromophenyl)]cyclopentadienylruthenium(II) **L3-Ru-(CO)$_2$Br** with a yield of 82%, whereas **L3-Ru-(CO)$_2$Br** was prepared in two-step synthesis from ligand **L3Br** with the triruthenium dodecacarbonyl cluster $Ru_3(CO)_{12}$, as previously described.[17,21] The synthesis of the complex **Ar$_5$L1-Ru-S1** was achieved through the fivefold Suzuki–Miyaura cross-coupling reaction of **L3-Ru-S1** with a large excess of 3,5-dimethylphenylboronic acid (4 equiv. per Br centre). The desired product resulting from five consecutive biaryl couplings was obtained in 52% yield which correspond to 88% per coupling reaction.[17] **L2H** was synthesised by direct palladium-catalysed five-fold arylation of cyclopentadiene according to a literature procedure.[22]

Absorption and Emission properties

Preliminary solubility and stability tests were performed in different solvents to evaluate the best medium for the photophysical characterisation of both complexes and ligands and THF was found to be the best choice. **L3-Ru-S1**, **Ar$_5$L1-Ru-S1** and their models **L1H**, **L3Br**, **S1K** and **S1Tl** were found to be stable at room temperature under ambient light for several days (Figure S1), while **L2H** and **L3-Ru-(CO)$_2$Br** showed limited stability. All the spectroscopic measurements were performed using freshly prepared solutions and investigated within 4 hours from preparation.

The absorption spectra of **Ar$_5$L1-Ru-S1** and its model ligands **L1H**, **L2H**, **S1K** and **S1Tl** are gathered in Figure 1 and the corresponding spectral data are collected in Table 1**. L1H** and **L2H** exhibit two bands in the regions 200-300 nm and 300-400 nm while **S1K** and **S1Tl** absorb only below 320 nm and show similar spectra. The molar absorption coefficient of **S1K** is slightly lower than that of **S1Tl** at higher energy. Surprisingly, the molar absorption coefficient of **Ar$_5$L1-Ru-S1** is much higher in the UV region (ε = 13.0×10^4 M^{-1}cm^{-1} at 267 nm) when compared to its ligands. Moreover, some new absorption features appear in the 400-500 nm range, indicative of metal-ligand interactions. A detailed theoretical analysis will discuss below these peculiar features, showing that a charge transfer transition from the metal to the π^* orbitals of the phenyl substituents of the cyclopentadienyl ligand is responsible for the intense absorption in the 250-350 nm region.

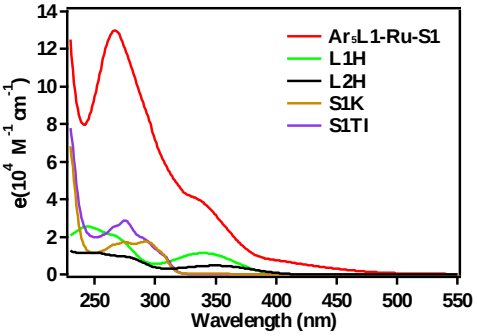

Figure 1. *Absorption spectra of the compounds **Ar$_5$L1-Ru-S1**, **L1H**, **L2H**, **S1K** and **S1TI** in THF solution at 298 K.*

Table 1. *Main absorption parameters in THF at 298 K.*

	λ_{max}, nm (ε_{max}, $\times 10^4$ $M^{-1}cm^{-1}$)		λ_{max}, nm (ε_{max}, $\times 10^4$ $M^{-1}cm^{-1}$)
L1H	245 (2.54), 339 (1.14)	**S1Tl**	275 (2.87)
L2H	349 (0.47)	**L3-Ru-(CO)$_2$Br**	283 (2.95), 338 (0.62)
L3Br	275 (3.59), 371 (0.39)	**Ar$_5$L1-Ru1-S1**	267 (13.0)
S1K	275 (1.72), 292 (1.75)	**L3-Ru-S1**	311 (3.71)

Figure 2 compares the emission spectra of **Ar$_5$L1-Ru-S1** and its models **L1H, L2H, S1K** and **S1Tl** in THF both at 298 K and 77 K. **L1H** shows a weak fluorescence (ϕ_{em} = 0.75%) at room temperature (298 K) with maximum at 450 nm in THF, which blue-shifts at 430 nm at low temperature (77 K). On the other hand, the fluorescence of **L2H** with maximum at 389 nm at 298 K, red-shifts by ca. 50 nm when moving to low temperature. **S1K** and **S1Tl** are weakly fluorescent at room temperature (ϕ_{em} = 2.44% for **S1K** and 0.69% for **S1Tl**), with an emission maximum at about 325 nm (Figure 2) at 298 K. At low temperature, an intense phosphorescence is observed in both compounds (Figure 2 and S2), with a vibronic progression of about 1300 cm^{-1} for **S1K** and 1400 cm^{-1} for **S1Tl**, which are consistent with the symmetric vibrational modes of the phenyl ring.

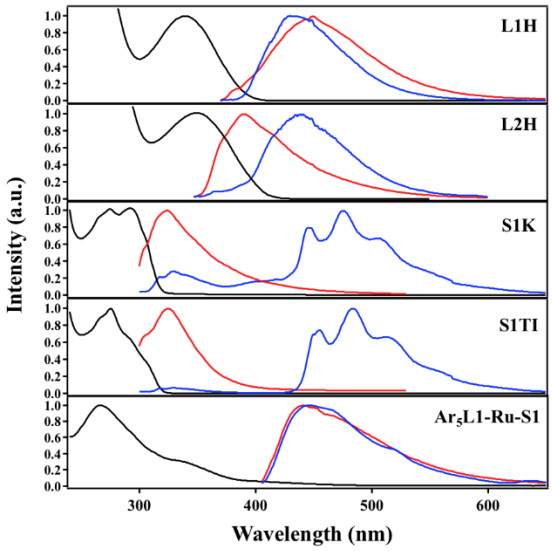

Figure 2. *Normalised absorption (black line) and emission spectra of* ***Ar$_5$L1-Ru-S1*** *and its related ligands/moieties* ***L1H***, ***L2H***, ***S1K*** *and* ***S1Tl*** *in deoxygenated (red line) THF at 298 K and in frozen solvent at 77 K (blue line). Excitation wavelengths are 340 nm, 310 nm and 360 nm for* ***L1H***, ***L2H*** *and* ***Ar$_5$L1-Ru-S1****, respectively, and 275 nm for* ***S1K*** *and* ***S1Tl****.*

The normalised absorption and excitation spectra of **L1H**, **L2H**, **L3Br**, **S1K** and **S1Tl** are gathered in Figure S3 (in THF at 298 K and 77 K). Except for **L2H**, the collected excitation spectra, are reasonably matched with the absorption profiles, corroborating the observed emission band. On the contrary, the poor match observed between absorption and excitation profiles of **L2H** may indicate limited stability of this compound.

Upon excitation at 360 nm, **Ar_5L1-Ru-S1** exhibits an emission spectrum with a broad band centred at ca. 440 nm under all conditions (Figure 2). To verify the occurrence of wavelength-dependent luminescence behaviour, emission maps were acquired at different excitation wavelengths, from 300 to 395 nm. Figure 3 collects such maps in deoxygenated THF solutions at 298 K, as well as in frozen matrix at 77 K. No significant shift of the emission maximum of **Ar_5L1- Ru-S1** is detected by varying the excitation wavelength at 298 K, whereas the intensity of the emission band changes following the absorption profile. On the other hand, at 77 K, a wavelength shift from 470 to 450 nm is observed when moving the excitation wavelength from the 300-345 nm to the 345-390 nm region, while the emission intensity remains almost constant. This observed different behaviour might indicate excited states of different nature which are no longer thermally equilibrated in frozen matrix. The emission quantum yield of **Ar_5L1-Ru-S1** is particularly low, i.e. 0.27% in air-equilibrated THF (Table 2).

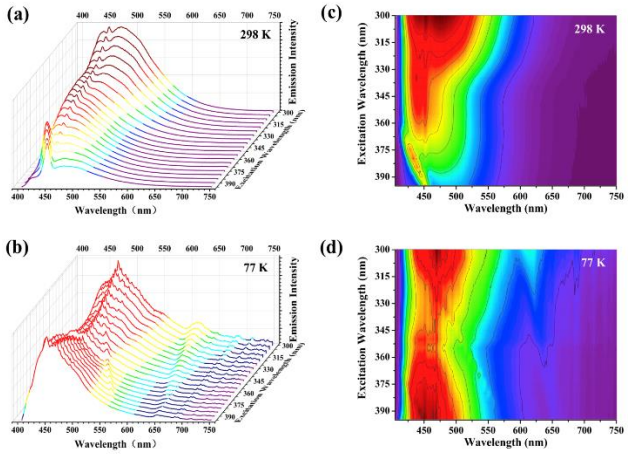

Figure 3. *Emission maps for **Ar_5L1-Ru-S1** in deoxygenated THF at 298 K (a and c) and in frozen THF at 77 K (b and d). The maps are depicted both as emission spectra distribution (left) and as contour plots (right). Excitation was moved from 300 nm to 395 nm with 5 nm steps. A spike due to the Raman signal is observed on the high energy side, which is unavoidable due to the weakness of the luminescence bands.*

Table 2. *Main emission parameters in THF.*

Table 2. Main emission parameters in THF.

	298 K[a]				77 K[b]	
	λ_{em}, nm	ϕ_{em}, %	τ, ns	τ*, ns	λ_{em}, nm	τ, ns (τ_{phos}, μs)
L1H	450	0.75	1.9	1.9	430	3.1
L2H	389	2.82	τ_1=1.0 (85%) τ_2=3.5 (15%)	τ_1=1.2 (86%) τ_2=5.2 (14%)	441	3.0
L3Br	477	0.30	/	/	464	3.2
L3-Ru-$(CO)_2$Br	468	2.67	/	/	468	3.5
S1K	325	2.44	3.0	4.0	329 (446, 476, 506)[c]	3.0 (1.4)[d]
S1Tl	325	0.69	3.5	4.9	330 (455, 483, 514)[c]	3.3 (1.2)[d]
Ar_5L1-Ru-S1	437	0.27	τ_1=1.1 (82%) τ_2=3.2 (18%)	τ_1=1.1 (82%) τ_2=3.6 (18%)	442	τ_1=1.8 (79%) τ_2=6.2 (21%)

[a] THF solution at 298 K; [b] THF glass at 77 K; *Lifetimes measured in deoxygenated THF solutions; [c] Phosphorescence features; [d] Phosphorescence lifetimes (μs).

In Figure S4 is reported the absorption spectrum of **L3-Ru-S1**, together with that of the related ligands and intermediates (**L3Br** and **L3-Ru-(CO)$_2$Br**) in THF solution. Compared to its reference compounds, **L3-Ru-S1** shows new absorption features in the region 300-360 nm, likely due to charge transfer transitions involving the ruthenium centre and the tripodal ligand.

In Figure S5 are collected the normalised absorption and emission spectra of **L3Br**, **L3-Ru-(CO)$_2$Br** and **L3-Ru-S1** in air-equilibrated and deoxygenated THF at 298 K and in frozen solvent at 77 K; the related absorption and emission parameters are collected in Table 1 and Table 2. **L3Br** exhibits a weak emission (ϕ_{em} = 0.30%) with a maximum around 470 nm in all conditions. **L3-Ru-(CO)$_2$Br** shows an emission spectrum similar to that of **L3Br**, with a peak at 468 nm at both 298 K and 77 K, but having emission quantum yield significantly higher (ϕ_{em} = 2.67%) than the precursor fragment. The target complex **L3-Ru-S1** was found to be virtually non-emissive both at room temperature and at 77K. Therefore, we carried out emission maps only for the intermediate complex **L3-Ru-(CO)$_2$Br**, which is a relatively strong emitter. Excitation wavelengths were tuned from 300 nm to 395 nm and the results are shown in Figure S6. Both at 298 K and 77 K, the emission maxima and the relative peak intensities change with the excitation wavelengths. An apparent dual emission is observed, with different features when exciting at 300 - 350 nm or 350 - 400 nm. We tentatively ascribe this behaviour to the presence of some free cyclopentadienyl ligand, which is preferentially excited at 300-350 nm and shows emission features similar to those observed for **L3Br** upon excitation in the same region and may come from partial decomposition of **L3-Ru-(CO)$_2$Br.**

Theoretical analysis

In order to rationalise the experimental data described above, we have carried out a computational analysis of the photophysical properties of the systems depicted in Scheme 2 by means of DFT and TD-DFT calculations (see experimental part).

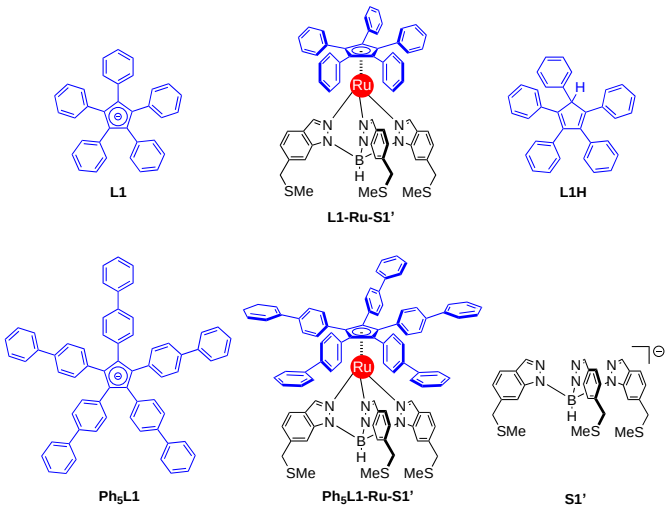

Scheme 2. *Structures of the calculated molecular rotors **L1-Ru-S1'** and **Ph$_5$L1-Ru-S1'**, along with their related ligands or fragments. In the calculated series was used **S1'** with three SMe substituents instead of the three SEt in **S1**.*

In Scheme 2, **L1-Ru-S1'** and **Ph_5L1-Ru-S1'** represent two model systems of **Ar_5L1-Ru-S1** where the **L1** and **Ph_5L1** upper ligands and the **S1** tripodal ligand are simplified for facilitating the calculations while still enabling a reliable rationalisation. They are respectively made of a cyclopentadienyl group substituted by five phenyls (**L1**) or five biphenyl (**Ph_5L1**) moieties whereas the tripodal ligand **S1'** exhibits three methyl substituents instead of the three ethyl in the synthesised tripodal ligand (**S1**). The phenyl or biphenyl substituents, even if the π-systems are not strictly parallel due to steric hindrance, can provide a partial π–delocalisation which can stabilise not only the negative charge of the cyclopentadienide core, but also additional charge resulting from light-induced electronic processes. In parallel, we have also investigated **L1H** and **S1'** and made additional comparisons with experimental data.

Ground-state geometries

The molecular geometries have been fully optimised by DFT methods, starting from the X-ray data of a parent complex of **Ar_5L1-Ru-S1**.[17] Since we changed the structure to simplify the molecule, we have modified the orientation of the phenyl groups of the upper parts and of the alkyl chain of the thioether legs in order to find two local energetically stable structures (see Experimental Section and Figure S12 A for the overlap between fragment of X-ray structure of a parent complex and calculated structures)**.** In Figure 4 (bottom) are depicted the geometries of **L1-Ru-S1'** and **Ph_5L1-Ru-S1'**. Upon full optimisation, a perfect superimposition of the two complexes is observed, except for the phenyl and biphenyl substituents of the two different cyclopentadienyl units (Figure S12 B). The average distance between the ruthenium centre and the five carbons of the cyclopentadienyl group are exactly the same in both ruthenium complexes (2.18 Å). Even the average distances between the three nitrogen atoms of the hydrotris(indazolyl)borate ligand directly coordinated to the ruthenium atom are the same (2.20 Å). On the other hand, as expected, **Ph_5L1** and **L1**, when analysed separately, exhibit geometries very different from those seen when complexed to the ruthenium centre. This illustrates the well-known steric hindrance between the pentaarylcyclopentadiene unit and the tripodal ligand.[18] Both have D_5 symmetry with the phenyls rotated out of the cyclopentadienyl plane for steric reasons (Figure 4, top).

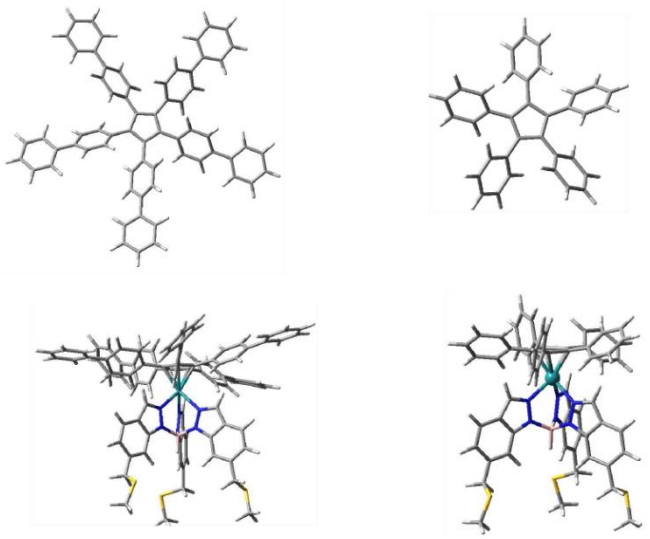

Figure 4. *Top: Geometries of the cyclopentadienide ligands **Ph_5L1** (left) and **L1** (right). Bottom: Geometries of the ruthenium complexes **Ph_5L1-Ru-S1'** (left) and **L1-Ru-S1'** (right)*

Absorption spectra

Figure 5 shows the calculated spectra of the two ruthenium complexes depicted in Scheme 2. **Ph_5L1-Ru-S1'** has one strongly dominating absorption feature in the UV with molar absorption coefficients comparable to the experimental values, i.e. between 10 and 12×10^4 $M^{-1}cm^{-1}$. The computational spectrum also reproduces well the experimental absorption features between 400 and 500 nm. The five lowest transitions of **Ph_5L1-Ru-S1'** are MLCT bands, i.e. from the ruthenium centre to the cyclopentadienyl ligand (**Ph_5L1**). Conversely, **L1-Ru-S1'** shows two distinct spectral domains (260-300 nm and 340-380 nm) with much lower molar absorption coefficients (maxima $2–3\times10^4$ $M^{-1}cm^{-1}$), which only partially matches the experimental absorption above 400 nm. The orbitals involved in the lowest energy transitions of **Ph_5L1-Ru-S1'** and **L1-Ru-S1'** (HOMO-LUMO orbitals, Figure 6 and Figure S7 respectively) clearly evidence charge transfer from the metal to the cyclopentadienyl ligand (MLCT). The HOMO is mainly located on the ruthenium centre and the LUMO is delocalised on the π^* of the **Ph_5L1** or **L1** phenyl ligands. These transitions peak at 492.6 and 481.1 nm respectively (Table 3).

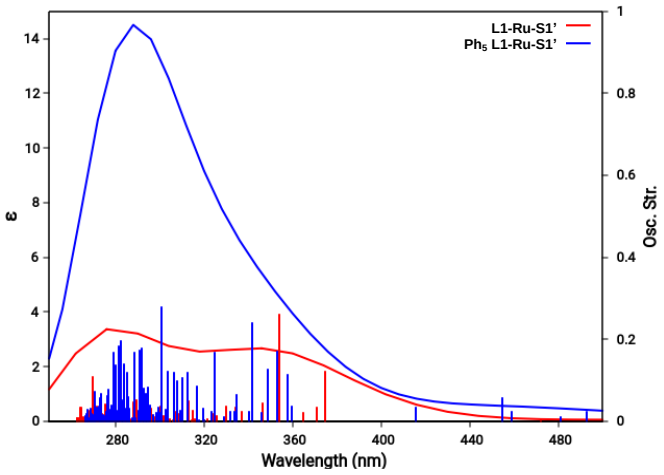

Figure 5. *Calculated absorption spectra (ε and oscillator strength) of **L1-Ru-S1'** (red line) and **Ph_5L1-Ru-S1'** (blue line).*

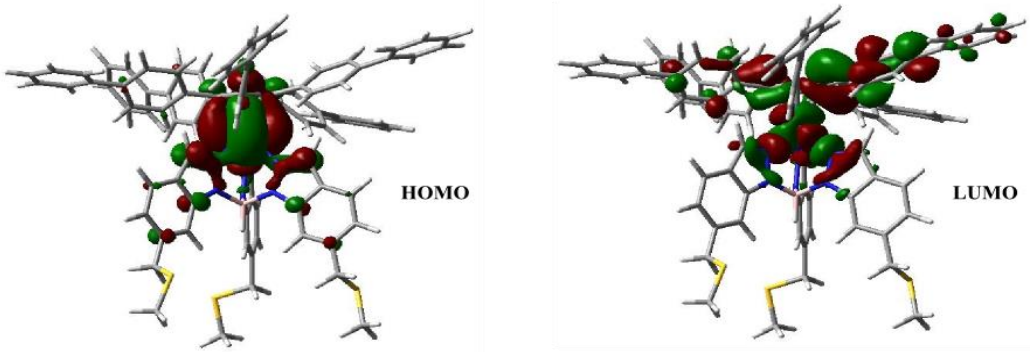

Figure 6. *HOMO – LUMO orbitals of **Ph_5L1-Ru-S1'** (Natural transition orbital, NTO) responsible for the lowest energy transition.*

Table 3. *Lowest calculated electronic transitions and related oscillator strength f.*

Structures	λ (nm)	*f*
Ph_5L1-Ru-S1'	492.6	0.0236
L1-Ru-S1'	481.1	0.0166
L1H	370.0	0.2618
L1	396.8	0.0017
Ph_5L1	438.4	0.0002
S1'	294.1	0.0312

The difference between the two ruthenium complexes can be attributed to the rotating parts **L1** and **Ph_5L1,** which have been studied independently (Scheme 2). **Ph_5L1** exhibits two spectral domains with high molar absorption coefficients (260-300 and 400-440 nm, 8–9×10^4 $M^{-1}cm^{-1}$), whereas **L1** has only one dominating absorption feature in the UV (320-380 nm) with a maximum molar absorption coefficient of 5×10^4 $M^{-1}cm^{-1}$ (Figure 7). In other words, absorption is more intense in the case of the larger and more delocalised system. The lowest π–π* transitions, a degenerate pair for each ligand due to their D_5 symmetry, are seen with peaks at 438.4 and 396.8 nm, respectively, with small oscillator strength. Picture of the orbitals involved in the transitions indicates a pseudo-charge transfer from the centre to the periphery (Figure S8 and Figure S9). The delocalisation plays an important role in the absorption spectra, but the features of the two ruthenium complexes are not significantly comparable with the spectra of the two different cyclopentadienyl ligands, as shown in Figure 6.

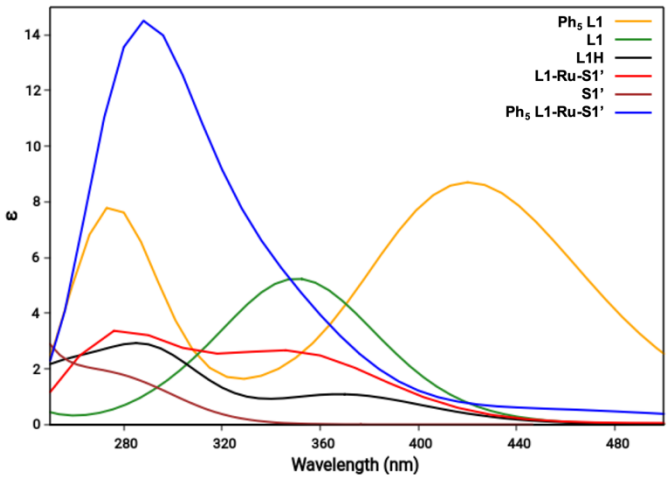

Figure 7. *Calculated absorption spectra of all the systems depicted in Scheme 2.*

L1H exhibits two bands in the regions 200-300 nm and 320-400 nm and **S1'** has the lowest energy transition below 320 nm (peak at 294.1 nm). The molar absorption coefficient of **S1'** is slightly lower than that of **L1** (Figure 7). The results are in good agreement with experiments even if **S1'** has been studied without a counterion. For **L1H**, the lowest energy transition is π–π* (HOMO-LUMO) and

peaks at 370 nm with an oscillator strength of 0.27 (Figure S10). It can be noticed that addition of hydrogen, with the loss of the negative charge of the cyclopentadienyl, makes absorption of **L1H** and **L1** very different (Figure 7, Figure S9 and Figure S10). **S1'** has two indazolyl cores that are closer to each other than the third. This is due to the interaction of a sulfur atom of the first arm with the aromatic group of the second. Interestingly, the $\pi-\pi^*$ transition is essentially related to a charge transfer from the arm not involved in the interaction with the other two (HOMO-LUMO orbitals in Figure S11).

CONCLUSION

The photophysical properties of two star-shaped molecular systems (**Ar_5L1-Ru-S1** and **L3-Ru-S1**) and their corresponding ligands / fragments have been investigated in THF solution. The photothermal stability tests for **Ar_5L1-Ru-S1** and **L3-Ru-S1** indicate that these two molecular rotors are stable in THF. New absorption features in the spectra of the complexes with respect to those of the corresponding ligands/fragments are attributed to ruthenium–based charge transfer transitions. A detailed theoretical investigation allowed to establish the role of the π^* delocalisation on the phenyl groups of the cyclopentadienyl ligand in the absorption transitions. Concerning the luminescence properties, no emission was found for **L3-Ru-S1**, while **Ar_5L1-Ru-S1** shows a weak emission with a quantum yield of 0.27% in THF. Overall, these rotors are viable platforms for the creation of photoactivable systems and our current efforts are devoted to this goal.

EXPERIMENTAL

Synthesis

All the synthetic details for the preparation of complexes **Ar_5L1-Ru-S1** and **L3-Ru-S1** as well as for the related ligands or intermediates **L2H**, **L3Br**, **S1K**, **S1Tl**, **L3-Ru-$(CO)_2$Br** were reported previously.[17,21,22]

Photophysical measurements

Spectrofluorimetric grade THF (Merck Uvasol®) was used without further treatments. The absorption spectra of the compounds were collected through a Perkin-Elmer Lambda 950 spectrophotometer by using pure THF as reference. Photoluminescence experiments in deoxygenated conditions were carried out into fluorimetric Suprasil quartz gas-tight cuvettes (1 cm), removing oxygen by bubbling argon for 20 minutes. An Edinburgh Instruments FLS920 spectrometer equipped with a Peltier-cooled Hamamatsu R928P photomultiplier tube (185−900 nm) and an Edinburgh 450 W xenon arc lamp (excitation light source) was used to record the emission spectra. The raw spectra were corrected by using a calibration curve supplied by the manufacturer. Photoluminescence quantum yields (ϕ_{em}) of the compounds in solutions were obtained from the corrected emission spectra by using an air-equilibrated water solution of quinine sulfate in 1 N H_2SO_4 as reference (ϕ_{em} = 0.546).[23] The excited state lifetimes (τ) were measured by means of a time-correlated single photon counting (TCSPC) HORIBA Jobin Yvon IBH FluoroHub equipment, with a TBX-05C Picosecond Photon Detection Module (300–850 nm) as the detector. Two excitation light sources (pulsed NanoLED) were used to collect the nanosecond range lifetimes, i.e. λ_{exc} = 368 nm (pulse duration < 1.4 ns) for **L1H**, **L2H**, **L3Br**, **L3-Ru-$(CO)_2$Br** and **Ar_5L1-Ru-S1**, λ_{exc} = 283 nm (pulse duration < 1.0 ns) for **S1K** and **S1Tl**. For the microsecond range lifetimes, a pulsed SpectraLED (λ_{exc} = 370 nm, FWHM = 11 nm) was used. The profiles of the luminescence

decays were analysed by means of the DAS6 Decay Analysis Software, and the quality of the fit was assessed with the χ^2 value (to be close to unity) and with the residuals randomly distributed along the time axis. Deconvolution of the instrument response function (IRF) has been applied in the fitting procedure. Mono-exponential (Model 1) and bi-exponential (Model 2) fitting functions were used:

Model 1: $F(t) = A + B\ exp(-t/\tau)$

Model 2: $F(t) = A + B_1\ exp(-t/\tau_1) + B_2\ exp(-t/\tau_2)$

For Model 2, the weighted amplitudes are expressed as: $f_i = B_i\,\tau_i / \Sigma_j B_j\,\tau_j$

The experimental decay traces and fitting results for the lifetime measurements in the ns range are collected in Table S1.

Low temperature (77 K) luminescence spectra were measured placing the sample solution in a 2 mm inner diameter quartz tube and inserting it into a special quartz cold finger Dewar flask filled with liquid nitrogen. Experimental uncertainties are estimated to be ±8% for τ determinations, ±20% for ϕ_{em}, and ±2 nm and ±5 nm for absorption and emission peaks, respectively.

Computational details

The X-ray structure of **Ar$_5$L1-Ru-S1** has been used to build the **L1-Ru-S1'** molecule. Figure S12A shows the overlap between the optimised molecule and a fragment of the X-ray structure of a parent complex. At this optimised molecule we added a second phenyl group to form the **Ph$_5$L1-Ru-S1'** structure. The X-ray structure shows that the second phenyl is attached in *para* and rotated out of the plane of the adjacent phenyl of ~±36° (see Scheme 3). Looking in detail in the X-ray structure of **Ph$_5$L1-Ru-S1**, both conformations with clockwise and counter-clockwise rotation exist in the crystal (Scheme 3) as expected for conformations with similar energies. For example, we tested that the energy difference between the structure where all phenyls are rotated clockwise and structure where they are rotated counter-clockwise is 0.06 kcal/mol. at the m06/6-31g(d,p) level. Consequently, we choose for all phenyls of **Ph$_5$L1-Ru-S1'** the clockwise rotation being confident that the electronic properties do not change. The starting geometry of **S1'** was obtained using the GMMX method included in Gaussian 16 package and that of **L1H** after testing different orientation of the phenyl groups.

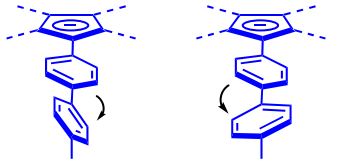

Scheme 3. *Relative rotation of adjacent phenyls.*

Density functional theory (DFT) calculations were carried out using the B.01 revision of the Gaussian16 program package[24] in combination with the M06 global-hybrid meta-GGA exchange-correlation functional.[25,26] The fully relativistic Stuttgart/Cologne energy-consistent pseudopotential with multielectron fit was used to replace the inner-core electrons of the ruthenium metal centre and was combined with the associated triple-ζ basis set (i.e., cc-pVTZ-PP basis).[27] The Pople 6-31G(d,p) basis was adopted for all other atoms to optimise the molecules and 6-31+G(d,p) for the single calculations TD-DFT.[28] All the optimisation procedures were performed using the polarisable continuum model (PCM) to simulate THF solvation effects.[29-31] Frequency calculations were always used to confirm that every stationary point found by potential-energy surface (no imaginary frequencies).

ACKNOWLEDGEMENTS

This work was supported by the CNRS, the University Paul Sabatier (Toulouse) and the Italian CNR (Project PHEEL). It has also received funding from the European Union's Horizon 2020 research and innovation program under the project MEMO, grant agreement No 766864 and from the JSPS KAKENHI grant in aid for Scientific Research on Innovative Areas "Molecular Engine (No.8006)" 18H05419 and the JSPS KAKENHI Grant-in-Aid for Challenging Research (20K21131). S.G. thanks the China Scholarship Council for his PhD fellowship (file n. 201706870014). Y.G. thanks the French Ministry of National Education for a PhD Fellowship. Dr Colin Martin is warmly acknowledged for his careful reading and improving of our manuscript.

REFERENCES

1 (*a*) R. P. Feynman, *Eng. Sci.*, 1960, **23**, 22-36; (b) V. Balzani, A. Credi and M. Venturi, *Molecular Devices and Machines. Concepts and Perspectives for the Nanoworld*, 2nd ed. Wiley-VCH, Weinheim, 2008; (*c*) S. Erbas-Cakmak, D. A. Leigh, C. T. McTernan and A. L. Nussbaumer, *Chem. Rev.*, 2015, **115**, 10081–10206.

2 V. Balzani, A. Credi, F. M. Raymo and J. F. Stoddart, *Angew. Chem. Int. Ed.*, 2000, **39**, 3348-3391.

3 V. Balzani, *Pure Appl. Chem.*, 2008, **80**, 1631-1650.

4 Y. B. Zheng, B. Kiraly and T. J. Huang, *Nanomedicine*, 2010, **5**, 1309-1312.

5 S. Ø. Scottwell and J. D. Crowley, *Chem. Commun.*, 2016, **52**, 2451-2464.

6 (a) J.-P. Sauvage, *Angew. Chem., Int. Ed.*, 2017, **56**, 11080-11093; (b) J. F. Stoddart, *Angew. Chem., Int. Ed.*, 2017, **56**, 11094-11125; (c) B. L. Feringa, *Angew. Chem., Int. Ed.*, 2017, **56**, 11060-11078.

7 J.-P. Collin, C. Dietrich-Buchecker, P. Gaviña, M. C. Jimenez-Molero and J.-P. Sauvage, *Acc. Chem. Res.*, 2001, **34**, 477-487.

8 (a) K. Kinbara, T. Muraoka and T. Aida, *Org. Biomol. Chem.*, 2008, **6**, 1871-1876; (b) A. G. Stewart, E. M. Laming, M. Sobti and D. Stock, *Curr. Opin. Struct. Biol.*, 2014, **25**, 40-48.

9 (a) M. Schliwa and G. Woehlke, *Nature*, 2003, **422**, 759-765; (b) S. Kassem, T. van Leeuwen, A. S. Lubbe, M. R. Wilson, B. L. Feringa and D. A. Leigh, *Chem. Soc. Rev.*, 2017, **46**, 2592-2621; (c) M. Baroncini, S. Silvi and A. Credi, *Chem. Rev.*, 2020, **120**, 200-268; (d) D. Dattler, G. Fuks, J. Heiser, E. Moulin, A. Perrot, X. Yao and N. Giuseppone, *Chem. Rev.*, 2020, **120**, 310-433; (e) V. García-López, D. Liu and J. M. Tour, *Chem. Rev.*, 2020, **120**, 79-124.

10 (a) K. H. Au Yeung, T. Kühne, F. Eisenhut, M. Kleinwächter, Y. Gisbert, R. Robles, N. Lorente, G. Cuniberti, C. Joachim, G. Rapenne, C. Kammerer and F. Moresco, *J. Phys. Chem. Lett.* 2020, **11**, 6892-6899; (b) S. Abid, Y. Gisbert, M. Kojima, N. Saffon-Merceron, J. Cuny, C. Kammerer and G. Rapenne, *Chem. Sci*. 2021, **12**, 4709-4721.

11 A. Goswami, S. Saha, P. K. Biswas and M. Schmittel, *Chem. Rev.*, 2020, **120**, 125-199.

12 (a) H. Iwamura and K. Mislow, *Acc. Chem. Res*., 1988, **21**, 175-182; (b) D. K. Frantz, A. Linden, K. K. Baldridge and J. S. Siegel, *J. Am. Chem. Soc.*, 2012, **134**, 1528-1535; (c) H. Ube, Y. Yasuda, H. Sato and M. Shionoya, *Nat. Commun.*, 2017, **8,** 1-6.

13 U. G. E. Perera, F. Ample, H. Kersell, Y. Zhang, G. Vives, J. Echeverria, M. Grisolia, G. Rapenne, C. Joachim and S.-W. Hla, *Nat. Nanotechnol.*, 2013, **8**, 46-51.

14 Y. Zhang, J. P. Calupitan, T. Rojas, R. Tumbleson, G. Erbland, C. Kammerer, T. M. Ajayi, S. Wang, L. C. Curtiss, A. T. Ngo, S. E. Ulloa, G. Rapenne and S.-W. Hla, *Nat. Commun.*, 2019, **10**, 3742.

15 (a) G. Vives, H.-P. Jacquot de Rouville, A. Carella, J.-P. Launay and G. Rapenne, *Chem. Soc. Rev.*, 2009, **38**, 1551-1561; (b) A. Carella, G. Vives, T. Cox, J. Jaud, G. Rapenne and J.-P. Launay, *Eur. J. Inorg. Chem.*, 2006, 980-987; (c) C. Kammerer and G. Rapenne, *Eur. J. Inorg. Chem.*, 2016, 2214-2226; (d) Y. Gisbert, S. Abid, G. Bertrand, N. Saffon-Merceron, C. Kammerer and G. Rapenne, *Chem. Commun.* 2019, **55**, 14689-14692.

16 (a) V. Balzani, A. Credi and M. Venturi, *Chem. Soc. Rev.*, 2009, **38**, 1542-1550; (b) S. Silvi, M. Venturi and A. Credi, *Chem. Commun.*, 2011, **47**, 2483-2489.

17 G. Erbland, S. Abid, Y. Gisbert, N. Saffon-Merceron, Y. Hashimoto, L. Andreoni, T. Guérin, C. Kammerer and G. Rapenne, C*hem. Eur. J.*, 2019, **25**, 16328-16339.
18 A. Carella, J. P. Launay, R. Poteau and G. Rapenne, *Chem. Eur. J.*, 2008, **14**, 8147-8156.
19 (a) Y. Wang and K. S. Schanze, *Inorg. Chem.*, 1994, **33**, 1354-1362; (b) G. J. Hollingsworth, K. S. K. Shin and J. I. Zink, *Inorg. Chem.*, 1990, **29**, 2501-2506; (c) M. S. Wrighton, L. Pdungsap and D. L. Morse, *J. Phys. Chem.*, 1975, **79**, 66-71; (d) H. Riesen, E. Krausz, W. Luginbühl, M. Biner, H. U. Güdel and A. Ludi, *J. Chem. Phys.*, 1992, **96**, 4131-4135; (e) M. Akiyama, Y. Tsuchiya, A. Ishii, M. Hasegawa, Y. Kurashige and K. Nozaki, *Chem. Asian J.*, 2018, **13**, 1902-1905.
20 (a) K. R. Bargawi, A. Llobet and T. J. Meyer, *J. Am. Chem. Soc.*, 1988, **110**, 7751-7759; (b) L. Huang, K. J. Seward, B. P. Sullivan, W. E. Jones, J. J. Mecholsky and W. J. Dressick, *Inorg. Chim. Acta*, 2000, **310**, 227-236; (c) M. Guelfi, F. Puntoriero, A. Arrigo, S. Serroni, M. Cifelli and G. Denti, *Inorg. Chim. Acta*, 2013, **398**, 19-27; (d) Q. H. Wei, Y. F. Lei, Y. N. Duan, F. N. Xiao, M. J. Li and G. N. Chen, *Dalton Trans.*, 2011, **40**, 11636-11642; (e) N. E. Katz, I. Romero, A. Llobet, T. Parella and J. Benet-Buchholz, *Eur. J. Inorg. Chem.*, 2005, 272-277.
21 G. Erbland, Y. Gisbert, G. Rapenne and C. Kammerer, *Eur. J. Org. Chem.*, 2018, 4731-4739.
22 G. Dyker, J. Heiermann, M. Miura, J.-I. Inoh, S. Pivsa-Art, T. Satoh and M. Nomura, *Chem. Eur. J.*, 2000, **6**, 3426-3433.
23 S. R. Meech and D. Phillips, *J. Photochem.*, 1983, **23**, 193-217.
24 M. J. Frisch, G. W. Trucks, H. B. Schlegel, G. E. Scuseria, M. A. Robb, J. R. Cheeseman, G. Scalmani, V. Barone, G. A. Petersson, H. Nakatsuji, X. Li, M. Caricato, A. V. Marenich, J. Bloino, B. G. Janesko, R. Gomperts, B. Mennucci, H. P. Hratchian, J. V. Ortiz, A. F. Izmaylov, J. L. Sonnenberg, D. Williams-Young, F. Ding, F. Lipparini, F. Egidi, J. Goings, B. Peng, A. Petrone, T. Henderson, D. Ranasinghe, V. G. Zakrzewski, J. Gao, N. Rega, G. Zheng, W. Liang, M. Hada, M. Ehara, K. Toyota, R. Fukuda, J. Hasegawa, M. Ishida, T. Nakajima, Y. Honda, O. Kitao, H. Nakai, T. Vreven, K. Throssell, J. A. Montgomery, Jr., J. E. Peralta, F. Ogliaro, M. J. Bearpark, J. J. Heyd, E. N. Brothers, K. N. Kudin, V. N. Staroverov, T. A. Keith, R. Kobayashi, J. Normand, K. Raghavachari, A. P. Rendell, J. C. Burant, S. S. Iyengar, J. Tomasi, M. Cossi, J. M. Millam, M. Klene, C. Adamo, R. Cammi, J. W. Ochterski, R. L. Martin, K. Morokuma, O. Farkas, J. B. Foresman and D. J. Fox, *Gaussian 16, Revision B.01*, Gaussian Inc., Wallingford, CT, USA, 2016.
25 Y. Zhao and D. G. Truhlar, *Theor. Chem. Acc,*. 2008, **120**, 215-241.
26 Y. Zhao and D. G. Truhlar, *Acc. Chem. Res.*, 2008, **41**, 157-167.
27 D. Figgen, K. A. Peterson, M. Dolg and H. Stoll, *J. Chem. Phys.*, 2009, **130**, 164108.
28 M. M. Francl, W. J. Pietro, W. J. Hehre, J. S. Binkley, M. S. Gordon, D. J. DeFrees and J. A. Pople, *J. Chem. Phys.*, 1982, **77**, 3654-3665.
29 J. Tomasi and M. Persico, *Chem. Rev.*, 1994, **94**, 2027-2094.
30 J. Tomasi, B. Mennucci and R. Cammi, *Chem. Rev.*, 2005, **105**, 2999-3093.
31 C. J. Cramer and D. G. Truhlar in *Continuum solvation models*, Springer, Dordrecht, Netherlands, 2002, pp. 1-80.